Provisional chapter

Pulsating Flow Effects on Hydrodynamics in a Desalination Membrane Filled with Spacers

Armando A. Soares, João Silva, Eliseu Monteiro and Abel Rouboa

Additional information is available at the end of the chapter

Abstract

A previously developed and validated two-dimensional computational fluid dynamics (CFD) model to study the hydrodynamics in a desalination membrane filled with spacers in zig-zag arrangements has been further developed to include the effects of a pulsating flow with the profile of a heartbeat. Numerical solutions were obtained with *Fluent* for pulsating laminar flows in channels filled with four different spacers and four lengths of cells. Hydrodynamics was investigated for unsteady state, using a characteristic function of a heartbeat, in order to study the influence of temporal variation in the hydrodynamic behavior. The results show the velocities distribution, streamlines, pressure drop and the wall shear stress on the impermeable wall of the membrane, for Reynolds numbers up to 100. The reduction in the distance between the filaments of the spacers, leads to the appearance of more active recirculation zones that can promote mass transfer and decreasing concentrations layers. On the other hand, this reduction increases the pressure drop and consequently the energy expended in the process. Further, the characteristic function of heartbeat demonstrates promising results, with regard to the energy consumption in the process and optimization of the recirculation zones.

Keywords: desalination, membrane, reverse osmosis, zig-zag spacers, heartbeat flow profile

1. Introduction

The planet has not only freshwater, but from the enormous volume of water available on our planet, only 3% is not salty. This resource is limited and finite, vital for the existence of life on earth and for the economic and social development [1].

The exploitation of natural water resources combined with the increase in the world population, the changes in the life style, the inefficient use of water and its contamination, among other factors, leads to scarcity of natural freshwater to respond the necessities of the population [2]. Due to these factors, the demand for potable water, has led to an increasing need to find new alternative sources of drinking water.

Desalination provides a good alternative to reduce the problem of the scarcity of drinking water, once it provides clean water which otherwise would not be accessible for agricultural, industrial and services supply [3, 4].

Membrane systems are widely used in water treatment processes. Depending on the pore size, membrane processes can be classified as microfiltration (MF), ultrafiltration (UF), nanofiltration (NF) and reverse osmosis (RO). The MF and UF are used to remove small colloidal particles and bacteria. For removal of viruses and large molecules such as proteins, the UF is only used. The NF and RO are capable of removing the smallest particles and components, like salts dissolved in water. In the case of RO, it is possible to remove almost all the components dissolved in the water [4].

The RO is the most used membrane separation method. This is applied at chemical, textile, petrochemical, electrochemical and paper industry, as well as in the treatment of municipal wastewaters [5]. But, the major application of RO process is the desalination of brackish and salty water to obtain potable water [6]. This is due to its versatility to operate over a wide range of feed water salinities, lower intake and pumping costs, minimal space requirements and operation at ambient temperatures [7]. Spiral wound modules (SWMs) have been largely used in industrial applications to obtain potable water, due to their low cost and high membrane area to volume ratio [8]. The performance of a SWM is affected by many factors such as leaf geometry (number and dimensions), spacers, fouling propensity, cleaning ability and operating conditions [9]. Despite several benefits of membrane technology over other separation techniques, the phenomena inherent to any membrane separation method are concentration polarization and fouling. As the filtration process occurs though the semipermeable membrane, the rejected impurities begin to accumulate on the membrane surface. After a certain period of time, a concentration layer is formed on the membrane surface due to the solute. This phenomenon, in which, the concentration of solute is higher in the vicinity of the membrane as compared with the observed in the fluid, is known as concentration polarization [10, 11]. This phenomenon can significantly affect the performance of the membrane, for example, the permeate water quality and productively are affected by fouling deposited on the membrane surface. On the other hand, from the literature it is well known that spacers are essential to separate the sheets of membranes in both spiral wound modules based thin rectangular channels (slits). Spacers are also important in the optimization of the mass transfer enhancement and pressure loss minimization [12, 13].

One important way by which the efficiency of module can be enhanced is to modify the hydrodynamics in membrane channel, which can be done by improving feed channel spacers design and using the unsteady state to induce a temporal variation in the feed velocity. This can prevent the accumulation of solutes near the membrane surface, thereby lowering the

concentration gradient between the bulk fluid and the membrane surface, and reducing fouling phenomenon [7].

The hydrodynamics inside the feed channel using computational fluid dynamics (CFD) has been investigated awhile. Cao et al. [14] investigated, trough CFD, the effect of three different cylindrical spacers arrangements: spacers touching the same channel wall, spacers touching opposite channel walls and spacers suspended in the channel. The flow simulations, in the spacer-filled channels, showed the distribution of velocity and turbulent kinetic energy as well as the detailed flow patterns. It was found that the presence of the spacer in the membrane is responsible for the local shear stress distribution on the membrane surface and improves the production of the eddy activities. It is also found that spacer configuration, geometry and position in the channel are crucial in the distribution of eddies and high shear stress on the membrane surface. The investigation also suggests that transverse spacer cylinders suspended in the channel are more desirable. Furthermore, decrease in the distance between transverse spacer cylinders can produce more active eddies and reduce the distance between shear stress peaks and consequently improve the mass transfer at the membrane surfaces. Besides that, it was demonstrated that the pressure drop is significantly increased by reduction in the distance between transverse cylinders which increase the operating costs. Schwinger et al. [15] perform CFD studies on how the use of spacers in membrane systems can affect its hydrodynamics. The flow fluid was studied in three different spacer configurations, the cavity, zig-zag, and submerged spacers. Were considered, in a cell, a single filament adjacent to the wall and centered in the channel for Reynolds numbers from 90 to 768 for different values of the length of the mesh and filament diameter. The results obtained show that the flow around the filament increases the wall shear stress and promotes the formation of large recirculation zones behind the filaments. Furthermore, under the same conditions, identical Reynolds number and filament diameter, a single filament adjacent to a membrane wall produced a larger recirculation zone than a single filament in the center of the channel. According to the authors, the utilization of the spacer in a SWM should enhance the mass transfer and reduce the accumulation of solute in the membrane surface while maintaining a low pressure loss along the channel. Saeed et al. [16] used a CFD tool to investigate the flow patterns associated with fluids within the membrane module. The effects on flow patterns through a spacer filled RO membrane with the secondary structure of the membranes (feed spacer filaments) at various angles with the inlet flow are analyzed. The results revealed that the alignment of the filaments in the direction of flow has a great influence on the generation of recirculation streams in channels filled with spacers. The optimization of the orientation of the filaments can lead to desirable recirculation patterns inside the modulus, and therefore, may increase the performance of the membrane. Sousa et al. [17] studied the hydrodynamics in a desalination membrane. CFD techniques were used to study the hydrodynamics of feed channels of a desalination membrane filled with elliptical spacers in zig-zag arrangements and transverse in relation to the flow, for four spacers and four cell lengths. They used *Re* values between 10 and 300 and the inlet velocity profiles are considered fully developed. The results showed that for *Re* values above 100, are formed recirculation zones downstream of the spacers. When the spacers are closer, there is a formation of more active recirculation zones. The authors state that these can increase the mass transfer and together with the pressure drop, there may be an

increase in process efficiency [17]. Amokrane et al. [18] used a model based on CFD which combines the fluid dynamics and the mass transfer in SWMs with zig-zag spacers, to investigate the impact of new spacers design. They affirm that zig-zag arrangement appears to have more advantages in the performance of RO membranes, in comparison, with submerged spacers. The results highlight that the incorporation of new spacer designs, such as elliptic and oval shapes, generates lower pressure drop (Δp) compared to conventional geometries. However, concentration polarization layer thickness, induced by elliptic and oval spacers, is higher compared to that of a circular spacer, while the mass transfer coefficient obtained with circular spacer is higher [18]. Al-Bastaki and Abbas [19] used a cyclic feed flow to improve the performance of membrane modules. The operation in cyclic mode generates flow instabilities, which in turn disturbs the fouling layer and increases the permeation rates. The cyclic operation can, however, need additional devices such as pulsation generator, oscillating pistons, and pneumatic valves. Lau et al. [20] performed a tri-dimensional study of the unsteady flow in order to optimize the spacer mesh angle for the SWM feed spacer. The results show that the presence of unsteady flow can significantly interrupt the development of the concentration of solute in the membrane surface. Filaments with different geometries and different angles may lead to different degrees of disruption in the concentration of the membrane layer. The filaments can be optimized in terms of concentration polarization and power consumption.

In the present investigation, a previously developed and validated two-dimensional CFD model to study the hydrodynamics in a desalination membrane filled with spacers in zig-zag arrangements [17], is further developed to include a characteristic function of a heartbeat within a cell of a semipermeable desalination membrane, in order to study the global and local impact of hydrodynamic behavior on the velocity, pressure drop, and wall shear stress for different spacer arrangements. The numerical approach used allows uncoupling of several phenomena and contributes to a better understanding of the mechanisms through which the shape of the flow profiles can affect membrane performance.

2. Governing equations and boundary conditions

An incompressible Newtonian fluid was used to simulate the bi-dimensional unsteady state flow in a feed channel of a SWM with zig-zag spacers (**Figure 1**). The governing equations are the continuity and Navier-Stokes equations. For a bi-dimensional flow, the governing equations can be written as:

Continuity equation

$$\frac{\partial v_x}{\partial x} + \frac{\partial v_y}{\partial y} = 0, \tag{1}$$

xx—Momentum equation

$$\rho\left(\frac{\partial v_x}{\partial t} + \frac{\partial}{\partial x}(v_x^2) + \frac{\partial}{\partial y}(v_x v_y)\right) = -\frac{\partial p}{\partial x} + 2\mu\frac{\partial}{\partial x}\left(\frac{\partial v_x}{\partial x}\right) + \mu\frac{\partial}{\partial y}\left(\frac{\partial v_x}{\partial y} + \frac{\partial v_y}{\partial x}\right) + \rho g_x \tag{2a}$$

and

yy—Momentum equation

$$\rho\left(\frac{\partial v_y}{\partial t}+\frac{\partial}{\partial x}(v_x v_y)+\frac{\partial}{\partial y}(v_y^2)\right)=-\frac{\partial p}{\partial y}+2\mu\frac{\partial}{\partial y}\left(\frac{\partial v_y}{\partial y}\right)+\mu\frac{\partial}{\partial x}\left(\frac{\partial v_x}{\partial y}+\frac{\partial v_y}{\partial x}\right)+\rho g_y \tag{2b}$$

where x and y are the spatial coordinates, ρ is the fluid density, μ is the dynamic viscosity, p is the static pressure, and g is the gravitational acceleration. The velocity components in x and y directions are v_x and v_y, respectively.

In the present study, the Reynolds number is defined as

$$Re=\frac{\rho\,\overline{v}\,h}{\mu} \tag{3}$$

where h is the height of the cell and $\overline{v}$ is the average inlet velocity in a cell, see **Figure 1**.

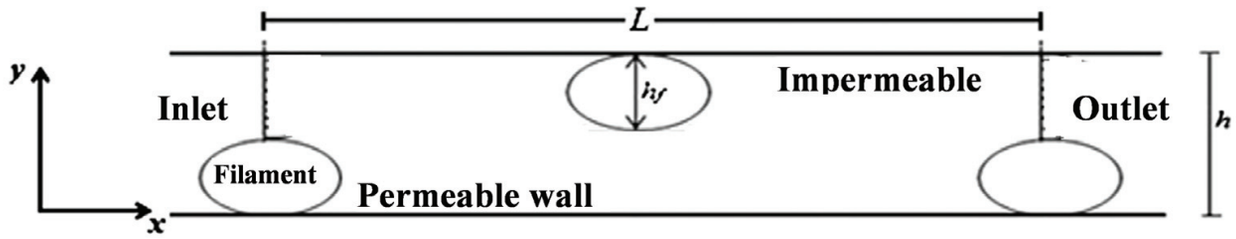

Figure 1. Schematic representation of a membrane cell with elliptical zig-zag filaments.

2.1. Inlet velocity profiles

In order to obtain a better numerical approach taking into account the flow periodicity, it was necessary to determine the velocity profile at the inlet and outlet of the cell [21]. As far as our knowledge in previous investigations, for example Refs. [8, 17, 22], it was considered a fully developed velocity profile at inlet. However, the velocity profiles between the filaments are not fully developed because there is no enough distance between filaments to allow the full development of the fluid flow. Therefore, for a given average velocity, the inlet velocity profile was obtained using the following procedure: for the value of *Re* studied, the corresponding average velocity is imposed at the inlet boundary. On the outlet boundary was considered the outflow option present in *Fluent*. With this condition, it is assumed that there are no diffusive fluxes of all variables at the exit in the flow direction, or a zero diffusion flux at the exit is expected to have a small impact on your flow solution.

For the case of impermeable walls, when the solution is achieved, the boundary condition at the inlet is replaced by the solution obtained for the velocity profile at the outlet boundary. This process was repeated until the differences between the inlet and outlet profiles were less than 0.15%. Similarly, in order to verify the permeability influence on the flow, a study was also done for a semipermeable membrane. To this, the bottom wall was considered permeable, with a constant flow rate of permeate. The value of permeate velocity (v_p) was 0.1 mm/s, value taken

from the literature [7, 8]. Since there is permeability, part of the flow is lost through the permeable wall and, thus for the conservation of mass principle be satisfied, the permeate flow rate has to be added to the outflow to obtain the inlet velocity profile. That is,

$$v_y(0, y) = v_y(L, y) \tag{4a}$$

$$v_x(0, y) = v_x(L, y) + \frac{L}{h - h_f} v_p(L, y) \tag{4b}$$

where the second term on the right-hand side of Eq. (4b) is the velocity profile in the outlet boundary obtained for the case of impermeable walls, when the imposed inlet flow rate is equal to the permeate flow rate.

The time-dependent velocity at the inlet was obtained from Doppler ultrasound images for a heartbeat, in the abdominal aorta, with a period of T = 1.53 s. **Figure 2** shows the normalized inlet velocity as function of time, $v_h(t)$, obtained from a polynomial fit of the Doppler data. Once given, the normalized velocity of the heartbeat was necessary to make an adjustment thereof, in order to encompass the typical velocities of a desalination membrane. Thus, the inlet velocity profile is given by

$$v_x(0, y, t) = v_x(0, y) \cdot v_h(t) \tag{5}$$

Then the normalized velocity $v_h(t)$ was multiplied by the velocity profiles, already determined for steady-state flow and so we obtained the inlet velocity profiles used in the present study, Eq. (5). For the impermeable membrane $v_x(0, y) = v_x(L, y)$.

The no-slip condition was applied at the wall boundaries.

Note that in the presence of permeability, it is needed to differentiate inlet and outlet profiles because some fluid is permeated through the permeable wall, see Eq. (4b).

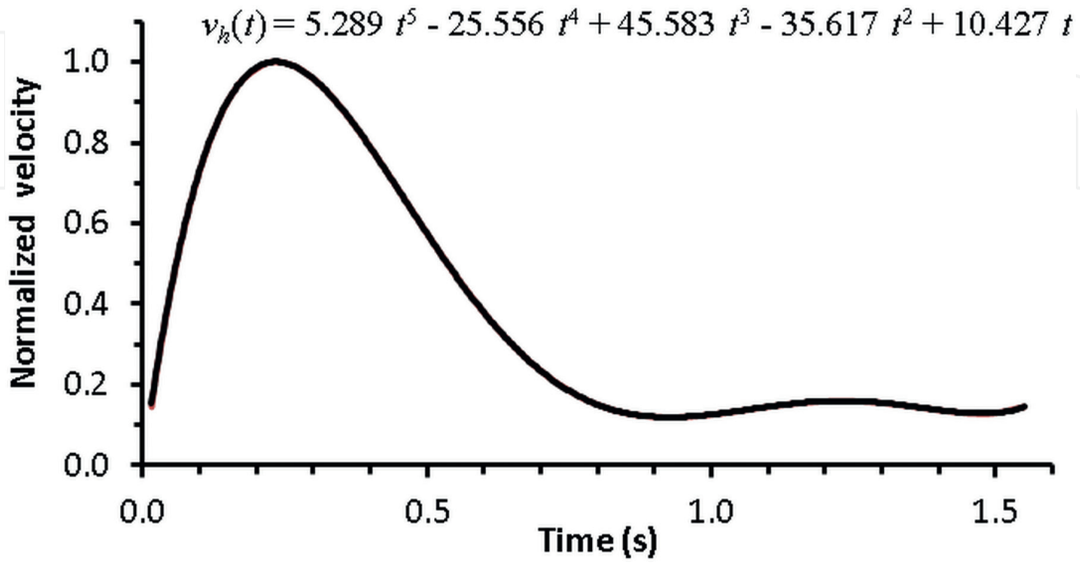

Figure 2. Normalized velocity for a heartbeat with a period T = 1.53 s.

3. Results and discussion

In this study, two-dimensional simulations using different feed channel geometries filled with spacers (different cells lengths and different shape of the elliptical filaments) were performed. We studied the impact on the velocity field, streamlines, average wall shear stress (*WSS*), and pressure drop for the cells lengths, $L = 4$, 6, 8, and 10 mm (**Figure 3**) and height of 0.7 mm. Four elliptical filaments configurations (*F*1, *F*2, *F*3, and *F*4) were also tested.

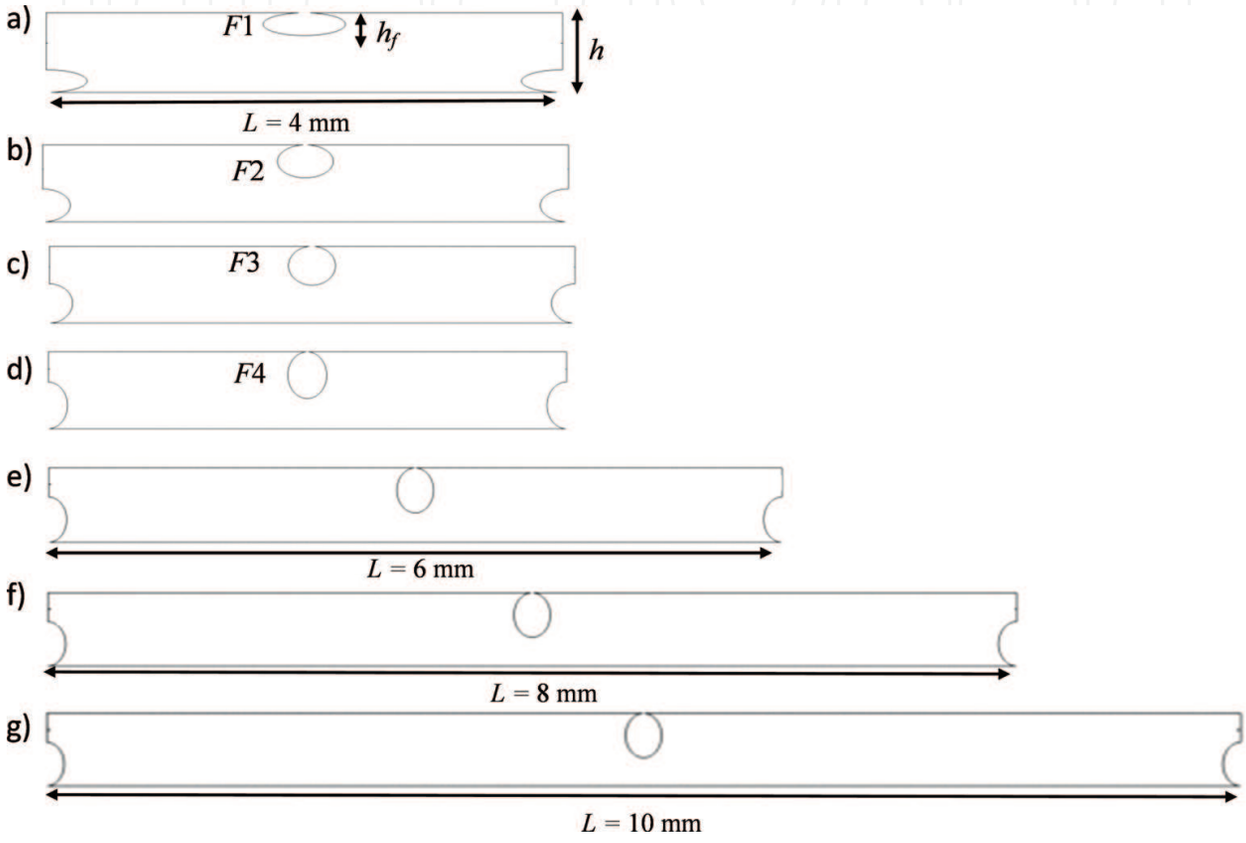

Figure 3. Cell filled with zig-zag spacers for (a) $L = 4$ mm and *F*1; (b) $L = 4$ mm and F2; (c) $L = 4$ mm and *F*3; (d) $L = 4$ mm and *F*4; (e) $L = 6$ mm and F4; (f) $L = 8$ mm and *F*4; (g) $L = 10$ mm and *F*4.

3.1. Inlet velocity profiles

Since for normal operation of the SWM, the velocity profiles inside the cell cannot be fully developed due to the filaments periodicity, so that the inlet profiles used in this study were determinate by the aforementioned procedure. As example, **Figure 4** shows the profiles determined for the four elliptical filaments with $L = 4$ and $Re = 100$, for the membrane with impermeable walls. Since permeable velocity is 0.1 mm/s, the inlet velocity profiles are practically unaltered by the permeability of the membrane when compared with the impermeable case, therefore they are not shown in **Figure 4**.

The width profiles decrease from *F*1 to *F*4 corresponding to the increase of flow obstruction by the spacers (**Figure 3**). Note that for the impermeable walls, the inlet and outlet profiles, for each configuration, are the same.

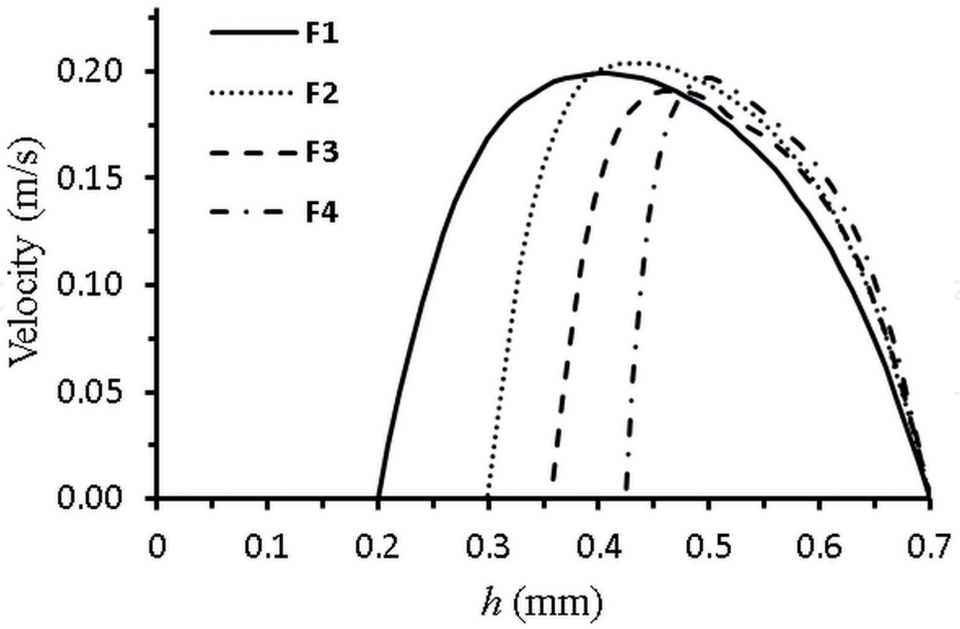

Figure 4. Inlet velocity profiles for *F*1, *F*2, *F*3, and *F*4, with *L* = 4 mm and *Re* = 100.

3.2. Velocity field

Figure 5 illustrates the velocity field for *Re* = 100 and *L* = 4 mm when *F*1 and *F*4 are used for both impermeable and semipermeable cases. A comparison between impermeable and semipermeable cases shows that the maximum velocity decreases by 0.2 and 3.1% for *F*1 and *F*4, respectively. This difference can be explained by the smaller useful area of permeable wall for *F*1 spacer, see Ref. [21]. Note that the average velocity in all cell is higher for *F*1 than for *F*4 because the inlet area is bigger for *F*1 spacer, however the average inlet velocity is the same for the two spacers.

From **Figure 5**, it can be seen that the well-known velocity behavior, that is, for each instant, the maximum velocity inside the membrane is located in the zones between the filament and the adjacent wall, for example Refs. [17, 23, 24]. This behavior is explained by the channel narrowing due to the spacers, with the consequent velocity increase to ensure the mass conservation. From general analysis of **Figure 5**, we can see that the maximum of velocity occurs at T/8. From this instant, velocity decreases until reaches approximately half of the period (T/2) and after that remains almost constant until the start of a new cycle. A more detailed analysis reveals that the permeability has a very little impact in the velocity. For instance, at 5T/8, velocity achieves the minimum value of 0.213 m/s for *F*1 to v_p = 0 mm/s while for v_p = 0.1 mm/s is 0.212 m/s. For *F*4, this value is 0.214 m/s for v_p = 0 mm/s and 0.208 m/s for v_p = 0.1 mm/s. **Figure 6** shows the velocity field for *F*1, *L* = 10 mm and impermeable membrane.

With increasing distance between the spacers, it is verified that for each instant, the average velocity within the cell decreases with increases of *L*, this observation are in line with previous studies (e.g. Ref. [17]). On the other hand, as in previous cases, the maximum velocity occurs at

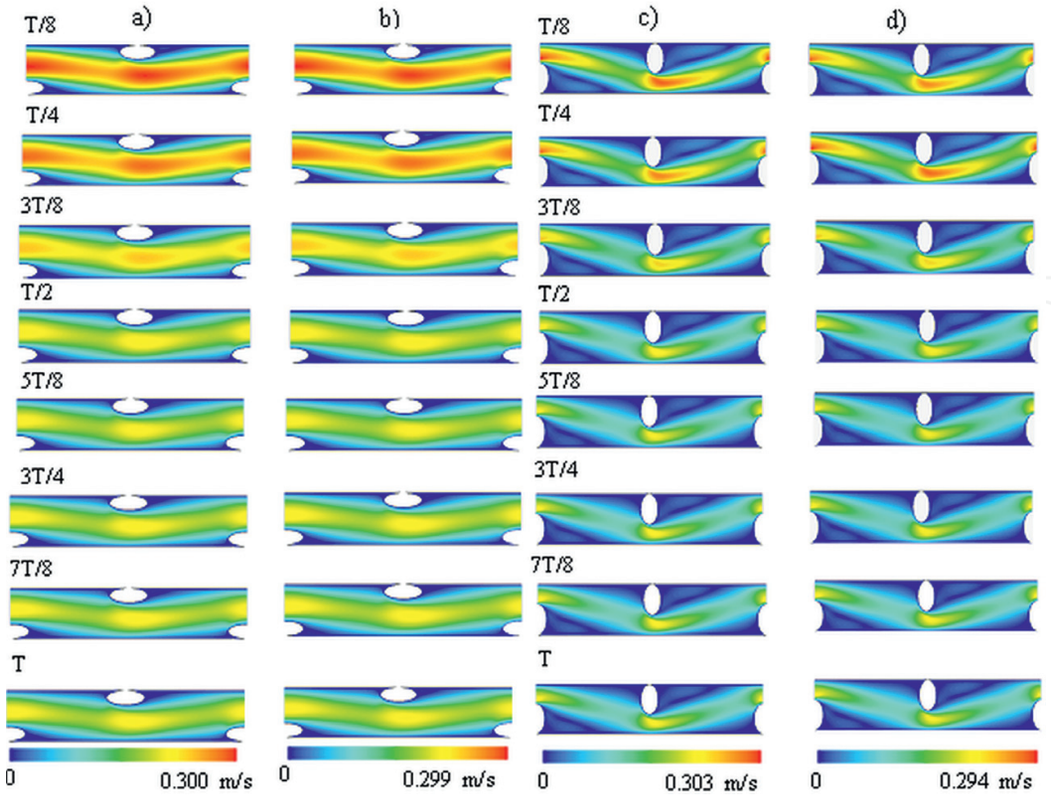

Figure 5. Velocity field during a period at t = T/8, T/4, 3T/8, T/2, 5T/8, 3T/4, 7T/8, and T, for L= 4 mm: (a) $F1$ and v_p = 0 mm/s; (b) $F1$ and v_p = 0.1 mm/s; (c) $F4$ and v_p = 0 mm/s; (d) $F4$ and v_p = 0.1 mm/s.

the t = T/8 and its value is 0.297 m/s. For both L = 10 mm and L = 4 mm, from T/2, looking only at the **Figures 5** and **6**, it appears that from that instant, the velocity remains constant. A more detailed analysis indicates that there are fluctuations, although small, and for t = 5T/8 is when the velocity takes the lowest value, equal to 0.213 m/s.

3.3. Average velocity inside the cell

Figure 7 shows the average velocity inside the cell for both cases, impermeable and semipermeable membrane, for a cell with length L = 4 mm, for all instants and spacers analyzed. The results presented are in concordance with **Figure 5**. The average velocity decreases from $F1$ to $F4$. It is also noteworthy that the highest average velocity occurs at instant T/8 undergoing a decrement up to the minimum value of average velocity at 5T/8. After 5T/8, the velocity remains almost constant but with small fluctuations in concordance with inlet velocity (**Figures 2**, **5**, and **6**).

A comparison between average velocities for impermeable and semipermeable cases also shows that the biggest difference is of 4.49% and occurs at 3T/8, for $F4$. The smallest difference between the two cases is verified for $F2$ at t = T/2, with a velocity decrease of 0.40%. On the other hand, for L = 10 mm, the corresponding biggest difference is of 4.13% for $F4$ at T/4 and smallest difference is of 1.71% for $F1$ at 7T/4, see **Figure 8**.

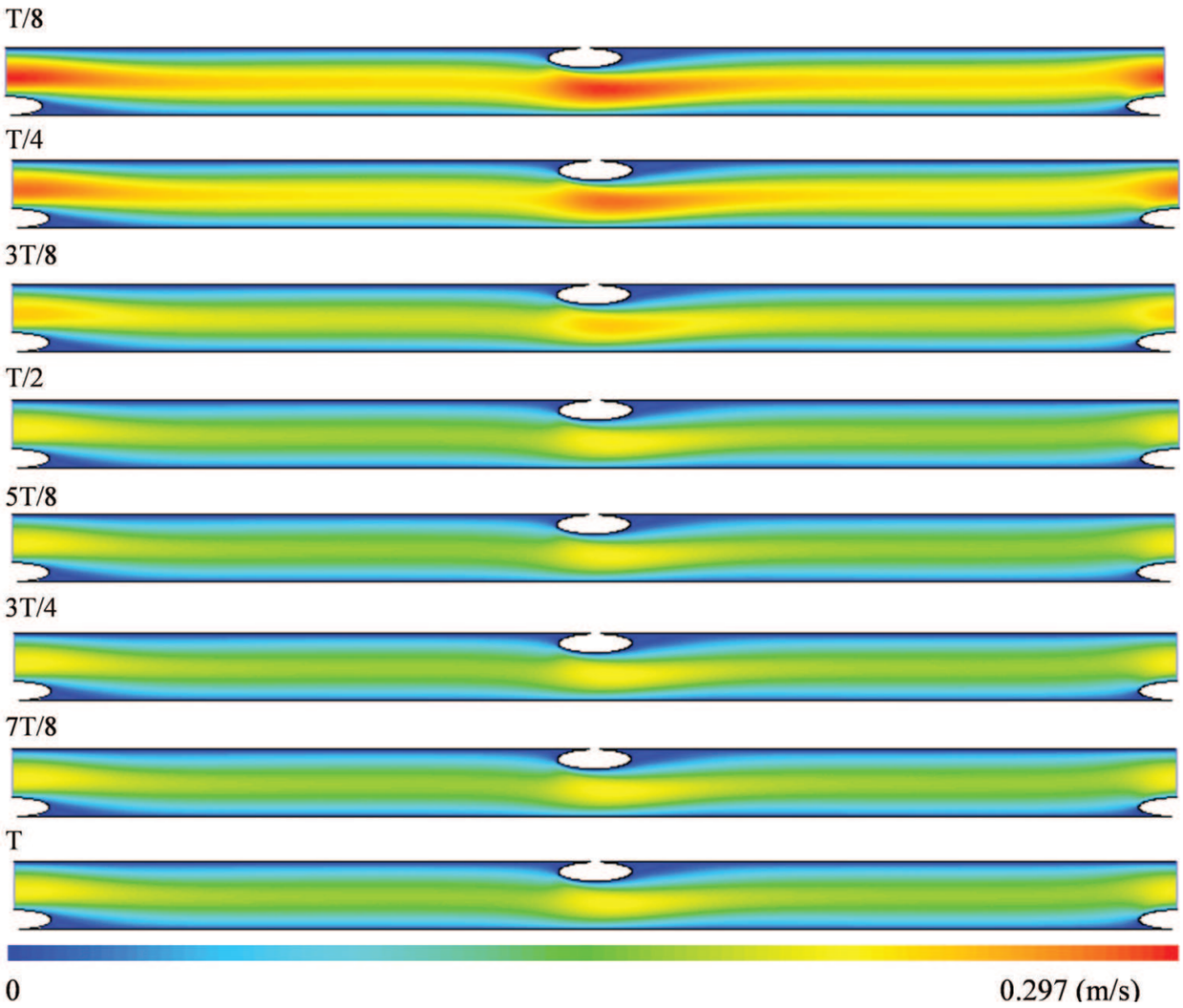

Figure 6. Velocity field during a period at t = T/8, T/4, 3T/8, T/2, 5T/8, 3T/4, 7T/8, and T, for L = 10 mm, $F1$ and v_p = 0 mm/s.

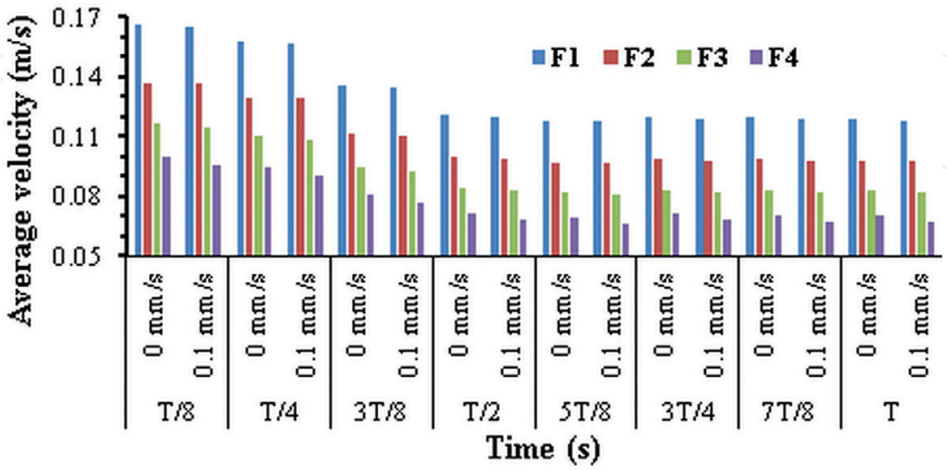

Figure 7. Average velocity during a period for L = 4 mm with v_p = 0 and 0.1 mm/s, for all spacers.

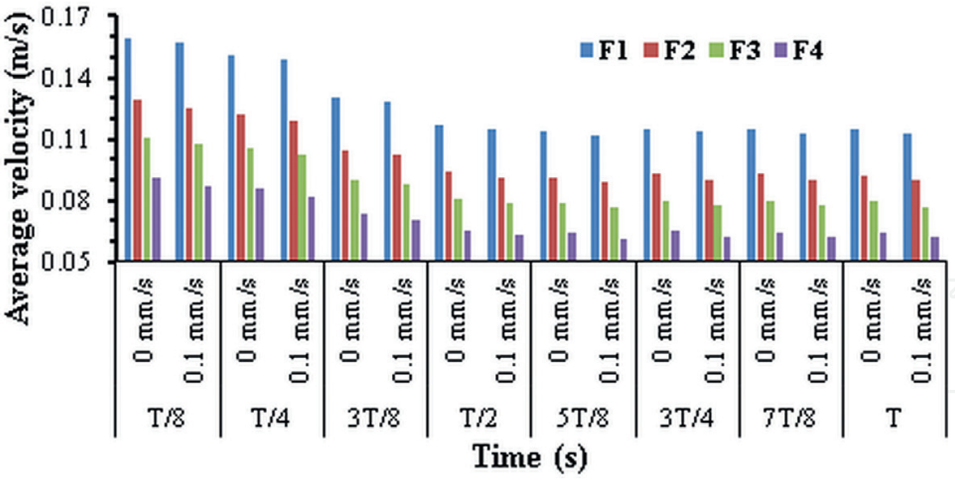

Figure 8. Average velocity during a period for L = 10 mm with v_p = 0 and 0.1 mm/s, for all spacers.

3.4. Streamlines

Figures 9 and **10** show the streamlines for L = 4 mm and the four types of spacers. Since the streamlines' differences for impermeable and semipermeable cases are insignificant, only the results for impermeable case are shown.

The recirculation zones are visible in all instants analyzed for all studied cell geometries. These zones are generally located downstream of the filaments, however, under specific conditions, small upstream recirculation zones can occur as shown in **Figure 9 (a)** at t = T/8 and **Figure 9 (d)** at t = T/8, T/4, and 5T/8. At t = T/8, the eddies occupy the largest area, since this instant is when the average velocity have the maximum value (**Figures 7** and **9**). From T/8 until T/2, the flow is in deceleration; consequently, the velocity decreases and the recirculation zones are reduced. After t = T/2, the velocity suffers small oscillations. These oscillations are responsible for the oscillations of the eddies length. This behavior is most easily seen in **Figure 9 (a)**. When t = T, it starts a new cycle and the fluid enters into a new stage of acceleration, leading to an increase in velocity which in turn causes a new increase in the recirculation zones. That behavior was observed in all geometrical configurations represented in **Figures 9** and **10**. Comparing the behavior of the different spacers, it should be noted that there is an increase in the area of eddies from *F*1 to *F*4. This increase can be explained by the shape of the spacer filaments. Note that *F*4 is the filament with biggest perpendicular area to the flow. In the present study, the distance between filaments is not sufficiently small to inhibit the growth of eddies. **Figure 10** shows the effects of the cell length, L, on the eddy length for the *F*4 configuration and maximum average velocity.

We can infer that the length between filaments has no influence on the eddies formation. Therefore, for all conditions studied, L does not affect the length of the recirculation zones.

The variation of the length eddies during a pulsatile flow modeled by a heartbeat shape combined with spacer arrangement may lead to better performance of the desalination membrane. Thus, the formation of desirable flow patterns within the membrane can lead to its better performance, which are in line with literature, for example, Saeed et al. [16].

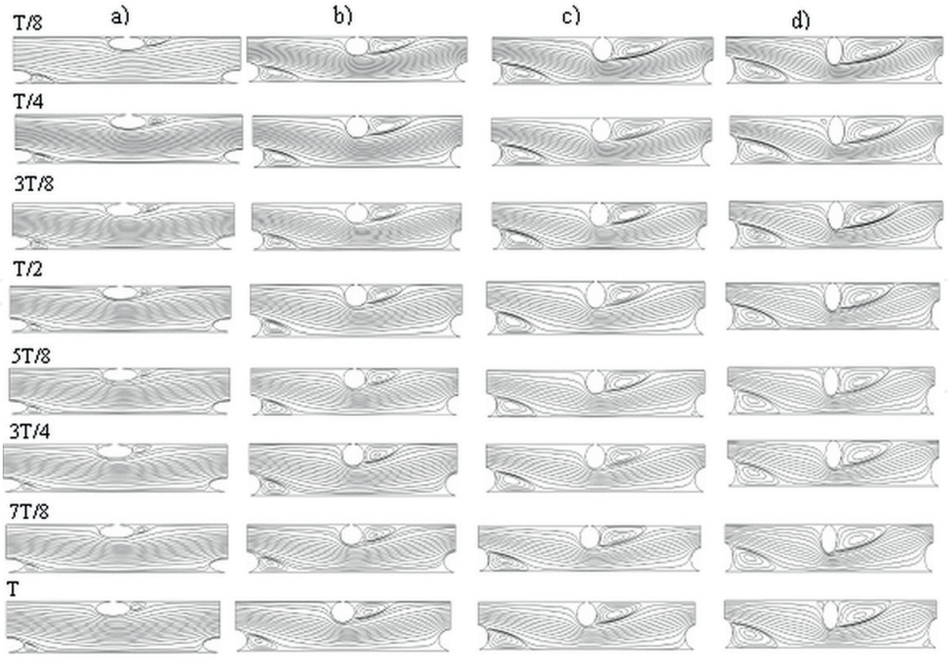

Figure 9. Streamlines during a period T at t = T/8, T/4, 3T/8, T/2, 5T/8, 3T/4, 7T/8 and T for v_p = 0 mm/s and L = 4 mm: (a) F1; (b) F2; (c) F3 and (d) F4.

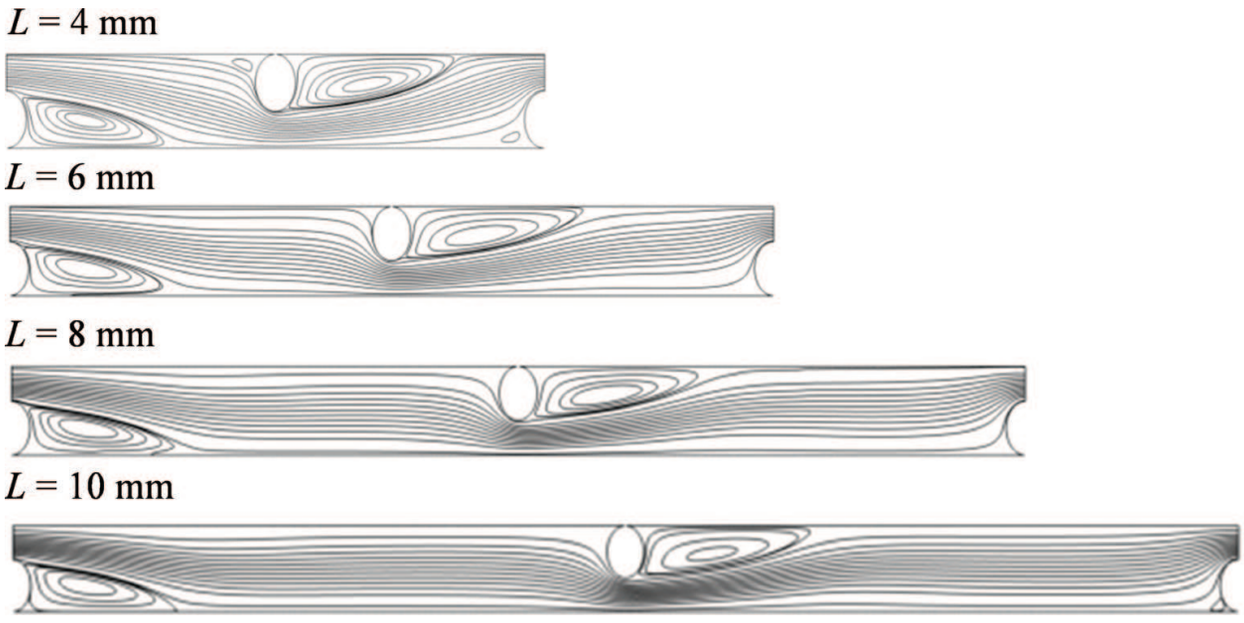

Figure 10. Streamlines at t = T/8 for $F4$, v_p = 0 mm/s and all values of L.

3.5. Pressure drop per length unit

Figure 11 shows the pressure drop per unit of length ($\Delta p/L$) in a cell membrane of desalination to the both cases, impermeable and semipermeable (v_p = 0.1 mm/s) for all spacers and L = 4 mm.

The maximum value of $\Delta p/L$ occurs at T/8 when the average velocity has its higher value. From there, the flow goes to a deceleration phase, and thus, there is a decrease in $\Delta p/L$ until t = 5T/8. As already mentioned, from that moment, there are small variations in the velocity, which lead

to the fluctuation in $\Delta p/L$ until t = T, when starts a new cycle which will lead to a further increase in $\Delta p/L$. However, $\Delta p/L$ has a reverse behavior to that observed for velocity, i.e., $\Delta p/L$ increases from $F1$ to $F4$. This increase can be explained by the geometric shape of the spacer filaments, that is, $F4$ is the spacer with bigger transverse area to the flow and consequently have the geometry with higher resistance to the flow, for that reason is needed a bigger spent of energy to overcome the resistance forces, due to the higher value of $\Delta p/L$.

On the other hand, v_p appears to have a small influence in $\Delta p/L$. The higher effect is verified for $F4$, when t = T/4, with a difference between the impermeable and semipermeable cases of 7.24%. The smallest influence is verified for $F2$, when t = 5T/8, with a difference of 2.45% between the two cases under study.

Figure 12 shows the pressure drop per unit of length ($\Delta p/L$) in a cell of the desalination membrane under impermeable and semipermeable (v_p = 0.1 mm/s) conditions for all spacers. From **Figure 12**, it is possible to infer that with the increase of the distance between the

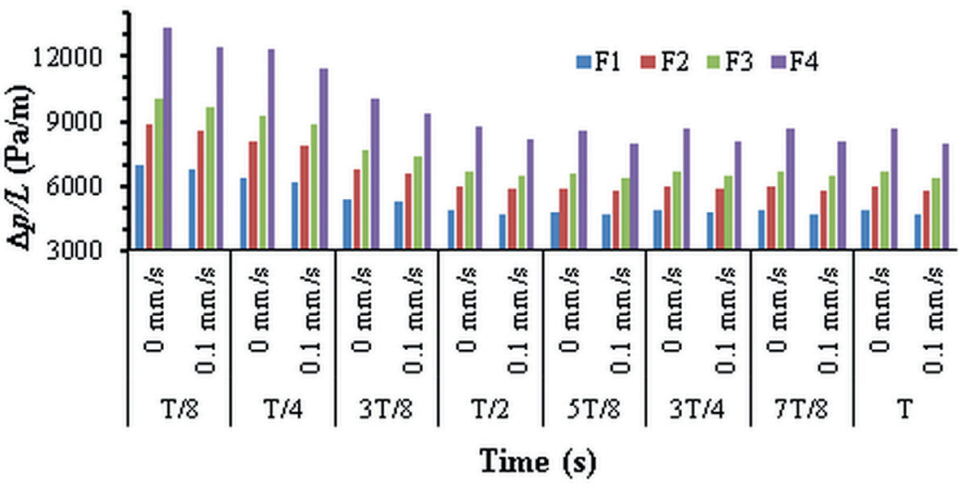

Figure 11. Pressure drop per unit length for L = 4 mm with v_p = 0 and 0.1 mm/s, for all spacers.

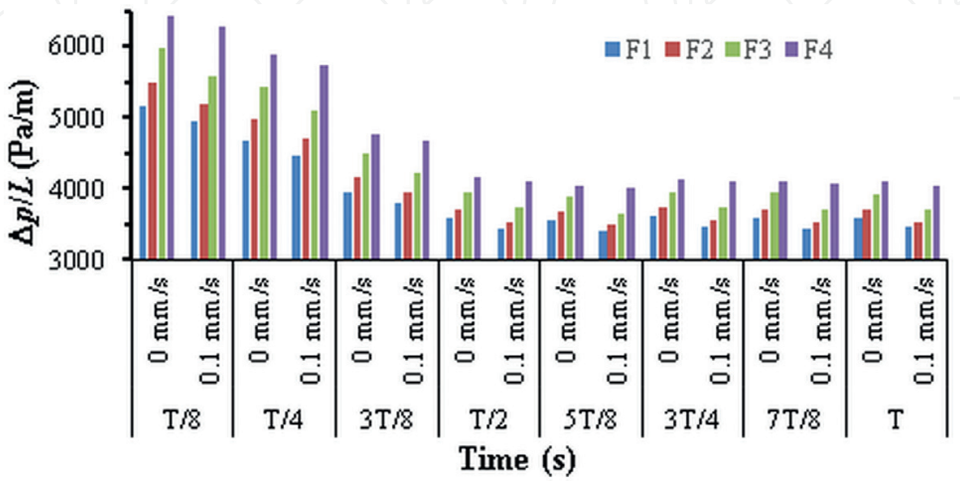

Figure 12. Pressure drop per unit length for L = 10 mm with v_p = 0 and 0.1 mm/s, for all spacers.

filaments there is a decrease in $\Delta p/L$. This phenomenon can be explained by the increased distance between filaments, that is, as the spacers are further apart, these offer a smaller resistance to the flow which is reflected in a smaller value of $\Delta p/L$ (see e.g. Ref. [17]).

The behaviors and conclusions seen in **Figure 11**, on the pressure drop per unit length, are also observed for this case, where $L = 10$ mm and for the other values of L not shown here. The main distinction between **Figures 11** and **12**, which is worth noting, is the difference in the values of $\Delta p/L$ for the different filaments. For instance for T/8 and $L = 4$ mm, the difference of $\Delta p/L$ between $F1$ and $F4$ is about five times higher than that for $L = 10$ mm, under the same conditions.

The results also show that v_p have a small influence on $\Delta p/L$. The differences observed are due to the shape of the filaments. The higher relative difference is verified for $F2$, when $t = T/2$, with a difference between the impermeable and semipermeable cases of 4.95%. The lowest relative difference is verified for $F4$, at $t = 5T/8$, with a difference of 1.01% between the two cases under study.

In general, an energy gain is expected when an inlet heartbeat function is used, compared to sinusoidal functions because in heartbeat function the flow keeps small fluctuations, at least, during half cycle, so in this case the pressure gradients developed during a cycle are smaller than that for a sinusoidal function.

3.6. Wall shear stresses per unit length

Figure 13 presents, for $L = 4$ mm, the average wall shear stress per unit length (WSS/L) in the upper wall (impermeable wall) of a desalination membrane for impermeable ($v_p = 0$ mm/s) and semipermeable cases ($v_p = 0.1$ mm/s). From **Figure 13**, one can see that for $v_p = 0.1$ mm/s, the values of WSS/L decrease from $F1$ to $F4$, at all instants analyzed. For the impermeable case,

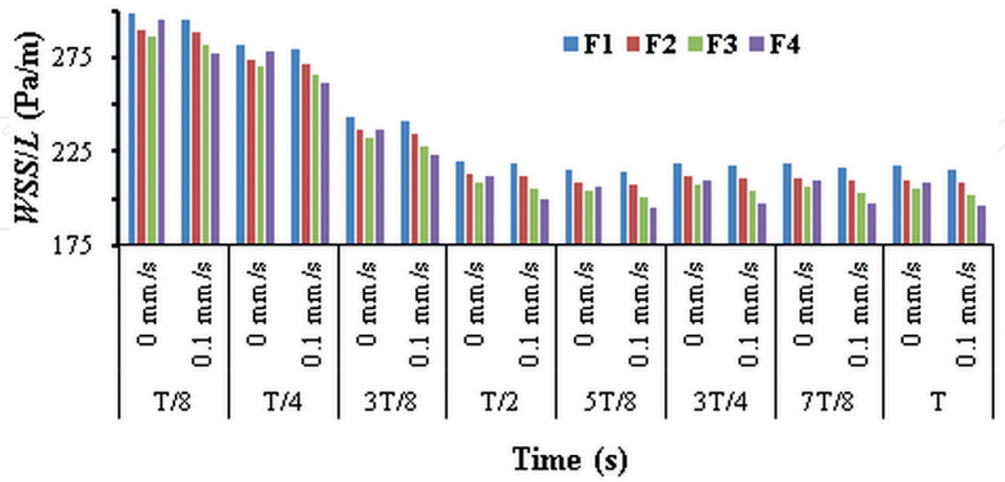

Figure 13. Average wall shear stress per unit length for $L = 4$ mm with $v_p = 0$ and 0.1 mm/s, for all spacers.

WSS/L only decreases from *F*1 to *F*3. The maximum values are verified at t = T/8, when the average velocity reaches its maximum values (**Figure 5**). From that instant *WSS/L* decreases in concordance with the average velocity. From T/2, the wall shear stress also presents small fluctuations.

For studied conditions, v_p appears to have small influence in *WSS/L*. The higher effect is verified for *F*4, at t = T/2, with a difference between the impermeable and semipermeable cases of 5.59%. The smaller influence occurs for *F*2, at t = T/2, with a difference between the two cases of 0.57%.

Figure 14 presents, for L = 10 mm, the average wall shear stress per unit length in the upper wall (impermeable wall) of a desalination membrane to the impermeable and semipermeable cases for conditions studied. In general, comparing **Figures 13** and **14**, the behavior of *WSS/L* is similar, with the exception of that for cell length (L = 10 mm), both impermeable and semipermeable cases show the same behavior of *WSS/L* with the type of spacers filaments, that is, for all instant, analyzed *WSS/L* decreases from *F*1 to *F*4.

The *WSS/L* for L = 10 mm also shows that permeability causes a decrease in *WSS/L*. The higher effect is verified for *F*4, at t = T/8, with a difference between the impermeable and semipermeable cases of 4.80%. The lesser influence is verified for *F*1, at t = 5T/8, with a difference between the two cases of 2.30%.

Comparing the results obtained by Cao et. al. [14] and Sousa et al. [17] with the present results, one can infer that the use of inlet flux with heartbeat profiles can benefit the membrane performance because the concentration polarization may be reduced, improving the mass transfer, once it dynamically changes the boundary layer concentrations and prevents clogging of the membrane surface.

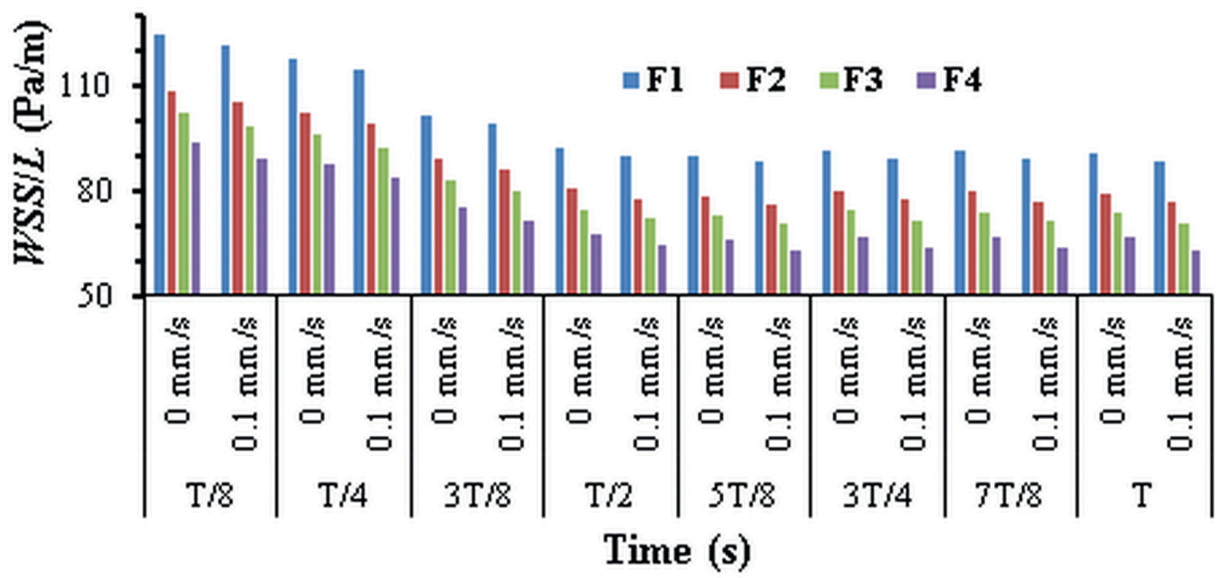

Figure 14. Average wall shear stress per unit length for L = 10 mm with v_p = 0 and 0.1 mm/s, for all spacers.

4. Conclusions

In this chapter, CFD techniques were used to study the hydrodynamics inside the feeding channel of a semipermeable membrane in spiral wound configuration. The main goal of this research was to investigate the effects of a pulsating flow with a profile of a heartbeat on the hydrodynamics of feed channels of a desalination membrane filled with spacers in zig-zag arrangements and transverse to the flow. Both membrane impermeable and semipermeable cases were analyzed. For the semipermeable case, we considered the membrane bottom wall with a typical permeation rate of 0.1 mm/s. The comparison between the two cases shows that the permeability has no significant influence on hydrodynamics. On the other hand, the permeability implies that there is a slight decrease in average velocity, Δp and *WSS*.

Due to the existence of the filaments in the cell, the velocity profiles are not fully developed. Thus, depending on spacer type (*F*1, *F*2, *F*3, or *F*4) and cell length, there is a different characteristic velocity profile. Analyzing the obtained velocity fields is possible to confirm that the maximum velocity occurs in the membrane region between the filament and the opposite wall. For *F*3 and *F*4, the shortest distance between consecutive filaments (L = 4 mm) provides eddies that sweep practically the entire membrane wall downstream of the filament, at t = T/8. The imposed eddies fluctuation by the pulsatile inflow can promote a reduction in the concentration polarization effect and reduce the concentration of solute at the membrane surface, which consequently increases the mass transfer. The reduction in the distance between the filaments increases *WSS*/*L*. The fluctuation in *WSS*/*L* can dynamically change the boundary layer concentrations and prevent clogging of the membrane surface. On the other hand, decreasing the distance between the filaments increases $\Delta p/L$ and this should increase the energy consumption. Thus, a combination of the distance between filaments, pulsatile inflow and $\Delta p/L$ is important to optimize separation process.

In summary, this study suggests that the inter-filaments length combined with the flow variation characteristic of a heartbeat can control the development of concentration polarization, and thus reduce the probability of fouling and energy consumption in the process, through an optimization of the recirculation zones.

Nomenclature

F	Filament
h	Cell height (m)
h_f	Filament height (m)
g	Gravitational acceleration (m s^{-2})
L	Cell length (m)
p	Static pressure (Pa)
Δp	Pressure drop (Pa)
Re	Reynolds number
$\overline{v}$	Average inlet velocity (m s^{-1})
v_p	Permeate velocity (m s^{-1})
$v_h(t)$	Normalized inlet velocity
v_x	Velocity component in x-direction (m s^{-1})
v_y	Velocity component in y-direction (m s^{-1})

x	Longitudinal rectangular coordinate (m)
y	Transverse rectangular coordinate (m)
Greek letters	
ρ	Fluid density (kg m^{-3})
μ	Dynamic viscosity (Pa s)

Acknowledgements

This work was supported by the Portuguese Foundation for Science and Technology under UID/SEM/04252/2013

Author details

Armando A. Soares[1,2], João Silva[1,2], Eliseu Monteiro[2,3] and Abel Rouboa[1,2,4]*

*Address all correspondence to: rouboa@utad.pt

1 UTAD, University of Trás-os-Montes and Alto Douro, Vila Real, Portugal

2 CIENER-INEGI/University of Porto, Porto, Portugal

3 C3i - Interdisciplinary Center for Research and Innovation, Polytechnic Institute of Portalegre, Portalegre, Portugal

4 Mechanical Engineering and Mechanics Department, University of Pennsylvania, Philadelphia, Pennsylvania, USA

References

[1] Tsiourtis NX. Desalination and the environment. Desalination. 2001;**141**(3):223–236. DOI: 10.1016/s0011-9164(01)85001-3

[2] Baalousha H. Desalination status in the Gaza Strip and its environmental impact. Desalination. 2006;**196**(1-3):1–12. DOI: 10.1016/j.desal.2005.12.009

[3] Marcovecchio MG, Mussati SF, Aguirre PA, Nicolás JS. Optimization of hybrid desalination processes including multi stage flash and reverse osmosis systems. Desalination. 2005;**182**(1):111–122. DOI: 10.1016/j.desal.2005.03.011

[4] Fritzmann C, Löwenberg J, Wintgens T, Melin T. State-of-the-art of reverse osmosis desalination. Desalination. 2007;**216**(1-3):1–76. DOI: 10.1016/j.desal.2006.12.009

[5] Bódalo-Santoyo A, Gomez-Carrasco JL, Gomez-Gomez E, Máximo-Martín MF, Hidalgo-Montesinos AM. Spiral-wound membrane reverse osmosis and the treatment of industrial effluents. Desalination. 2004;**160**(2):151–158. DOI: 10.1016/S0011-9164(04)90005-7

[6] Wangnick K. IDA Worldwide Desalting Plants Inventory. Report No. 17 ed. Gnarrenburg, Germany: Wangnick Consulting GMBH; 2002

[7] Shakaib M. Pressure and concentration gradients in membrane feed channels: Numerical and experimental investigations [thesis]. Karachi, Pakistan: University of Engineering and Technology; 2008. p. 271. Available from: http://prr.hec.gov.pk/Thesis/353S.pdf

[8] Geraldes V, Semião V, Pinho MN. Flow management in nanofiltration spiral wound modules with ladder-type spacers. Journal of Membrane Science. 2002;**203**(1.2):87–102. DOI: 10.1016/s0376-7388(01)00753-0

[9] Schwinge J, Neal PR, Wiley DE, Fletcher DF, Fane AG. Spiral wound modules and spacers: Review and analysis. Journal of Membrane Science. 2004;**242**(1-2):129–153. DOI: 10.1016/j.memsci.2003.09.031

[10] Baker RW. Membrane Technology and Applications. 2nd ed. Menlo Park, CA: John Wiley & Sons, Ltd; 2004. p. 538. DOI: 10.1002/0470020393

[11] Kim S, Hoek EMV. Modeling concentration polarization in reverse osmosis processes. Desalination. 2005;**186**(1-3):111–128. DOI: 10.1016/j.desal.2005.05.017

[12] Zimmerer CC, Kottke V. Effects of spacer geometry on pressure drop,mass transfer, mixing behavior, and residence time distribution. Desalination. 1996;**104**(1-2):129–134. DOI: 10.1016/0011-9164(96)00035-5

[13] Ahmad AL, Lau KK. Impact of different spacer filaments geometries on 2D unsteady hydrodynamics and concentration polarization in spiral wound membrane. Journal of Membrane Science. 2006;**286**(1-2):77–92. DOI: 10.1016/j.memsci.2005.06.056

[14] Cao Z, Wiley DE, Fane AG. CFD simulations of net-type turbulence promoters in a narrow channel. Journal of Membrane Science. 2001;**185**(2):157–176. DOI: 10.1016/S0376-7388(00)00643-8

[15] Schwinge J, Wiley DE, Fletcher DF. Simulation of the flow around spacer filaments between channel walls. 1. Hydrodynamics. Industrial & Engineering Chemistry Research. 2002;**41**(12):2977–2987. DOI: 10.1021/ie010588y

[16] Saeed A, Vuthaluru R, Yang Y, Vuthaluru HB. Effect of feed spacer arrangement on flow dynamics through spacer filled membranes. Desalination. 2012;**285**:163–169. DOI: 10.1016/j.desal.2011.09.050

[17] Sousa P, Soares A, Monteiro E, Rouboa A. A CFD study of the hydrodynamics in a desalination membrane filled with spacers. Desalination. 2014;**349**:22–30. DOI: 10.1016/j.desal.2014.06.019

[18] Amokrane M, Sadaouia D, Dudeckb M, Koutsouc CP. New spacer designs for the performance improvement of the zigzag spacer configuration in spiral-wound membrane modules. Desalination and Water Treatment. 2015;**57**(12):5266–5274. DOI: 10.1080/19443994.2015.1022003

[19] Al-Bastaki N, Abbas A. Use of fluid instabilities to enhance membrane performance: a review. Desalination. 2001;**136**(1-3):255–262. DOI: 10.1016/S0011-9164(01)00188-6

[20] Lau KK, Bakar AMZ, Ahmad AL, Murugesan T. Feed spacer mesh angle: 3D modeling, simulation and optimization based on unsteady hydrodynamic in spiral wound membrane channel. Journal of Membrane Science. 2009;**343**(1):16–33. DOI: 10.1016/j.memsci.2009.07.001

[21] Silva JC, Soares AA, Rouboa A. A numerical study of the hydrodynamics in feed channels of spiral-wound membrane modules. MEFTE. 2014; 227–232. In: APMTAC, editor. MEFTE 2014—V Conferência Nacional de Mecânica dos Fluidos, Termodinâmica e Energia; 11-12 Set 2014; Porto, Portugal. Porto: FEUP; 2014. p. 227–232

[22] Subramani A, Kim S, Hoek E. Pressure, flow, and concentration profiles in open and spacer-filled membrane channels. Journal of Membrane Science. 2006;**277**(1):7–17. DOI: 10.1016/j.memsci.2005.10.021

[23] Fimbres-Weihs GA, Wiley DE. Review of 3D CFD modeling of flow and mass transfer in narrow spacer-filled channels in membrane modules. Chemical Engineering and Processing: Process Intensification. 2010;**49**(7):759–781. DOI: 10.1016/j.cep.2010.01.007

[24] Radu AI, Bergwerff L, Loosdrecht MCM, Picioreanu C. A two-dimensional mechanistic model for scaling in spiral wound membrane systems. Chemical Engineering Journal. 2014;**241**(1):77–91. DOI: 10.1016/j.cej.2013.12.021

IntechOpen